Earth's Future

RESEARCH ARTICLE
10.1029/2022EF003397

Projected Changes in the Pattern of Spatially Compounding Drought and Pluvial Events Over Eastern China Under a Warming Climate

Huijiao Chen[1], Shuo Wang[1,2], Jinxin Zhu[3], and Dagang Wang[3]

[1]Department of Land Surveying and Geo-Informatics, Research Institute for Land and Space, The Hong Kong Polytechnic University, Hong Kong, China, [2]Shenzhen Research Institute, The Hong Kong Polytechnic University, Shenzhen, China, [3]School of Geography and Planning, Sun Yat-sen University, Guangzhou, China

Abstract The simultaneous occurrence of droughts and floods in neighboring regions amplifies the threats posed by droughts and floods individually. Nonetheless, few studies have been conducted to investigate the simultaneous occurrence of drought and flood events. Here we explore the spatiotemporal characteristics and the shift pattern of droughts and pluvials over Eastern China from a three-dimensional perspective, using the self-calibrated Palmer Drought Severity Index and the Climate Research Unit data set as well as four regional climate model simulations. We find that Eastern China experienced droughts and pluvials simultaneously in different locations during boreal summer, and it is projected to simultaneously experience more frequent and more intense droughts and pluvials under a warming climate. Specifically, we investigate the pattern of more pluvials in Southeast China and more droughts in Northeast China for the historical period of 1975–2004. This pattern dynamically evolves under climate warming: the pluvial-dominated regime shifts from Southeast to Northeast China, while the drought-dominated regime shifts from Northeast to Southeast China. The weakening strength of the western Pacific subtropical high and a northward displacement of the monsoon rain belt may both contribute to the pattern of more pluvials in Northeast China and more droughts in Southeast China. These findings provide insights into the development of adaptation strategies and emergency response plans for enhancing society's resilience to the spatial co-occurrence of dry and wet extremes.

Plain Language Summary The spatial co-occurrence of drought and flood events has been receiving widespread attention in recent years since the superimposed condition of drought and flood has brought unprecedented challenges to disaster prevention, mitigation, and relief work. Eastern China is prone to droughts and floods, but their spatial interconnections are not yet well understood. Thus, we explore the historical evolution and the future change of simultaneous occurrence of droughts and floods over Eastern China under a warming climate. The spatial co-occurrence of droughts and floods is projected to affect more land areas and become more frequent as climate warms. Eastern China experienced a pattern of more floods in Southeast China and more droughts in Northeast China during 1975–2004. We find that droughts tend to become more intense in Southeast China and the severity of floods is expected to increase in the northern region of East China, resulting in a shift pattern of more droughts in Southeast China and more floods in Northeast China. The shift pattern may be attributed to the weakening of western Pacific subtropical high strength and a northward displacement of the monsoon rain band in a changing climate.

Key Points:

- Eastern China is projected to experience more frequent and more intense droughts and pluvials simultaneously
- The spatial pattern of more pluvials in Southeast China and more droughts in Northeast China is expected to become an opposite pattern under a warming climate
- The weakening strength of the western Pacific subtropical high and a northward displacement of the monsoon rain belt may contribute to the pattern of more pluvials in Northeast China and more droughts in Southeast China

Supporting Information:

Supporting Information may be found in the online version of this article.

Correspondence to:

S. Wang,
shuo.s.wang@polyu.edu.hk

Citation:

Chen, H., Wang, S., Zhu, J., & Wang, D. (2023). Projected changes in the pattern of spatially compounding drought and pluvial events over Eastern China under a warming climate. *Earth's Future*, *11*, e2022EF003397. https://doi.org/10.1029/2022EF003397

Received 30 NOV 2022
Accepted 21 APR 2023

Author Contributions:

Conceptualization: Shuo Wang
Data curation: Huijiao Chen
Formal analysis: Huijiao Chen, Jinxin Zhu
Funding acquisition: Shuo Wang
Investigation: Shuo Wang
Methodology: Huijiao Chen, Shuo Wang
Project Administration: Shuo Wang
Resources: Shuo Wang
Software: Huijiao Chen

1. Introduction

Droughts and floods have been regarded as the costliest natural hazards with widespread impacts (Chen, Wang, & Wang, 2020; Dong et al., 2011; Qing et al., 2022; Schumann et al., 2016; Trenberth et al., 2014). The frequencies of both droughts and floods have doubled in the recent 20 years (2000−2019) compared to the period of 1980–1999 globally (UNDRR & CRED, 2019). Hydrometeorological extremes have been increasing in recent decades, which can be attributed to the combined influence of increased variability in precipitation (Wu et al., 2019; W. Zhang et al., 2021) and human activities, leading to the increasing water-related disasters around the world (Duan et al., 2022).

Drought and pluvial (flood) events can be spatially interconnected since a shift in atmospheric circulation can trigger droughts in one region while causing floods in a neighboring region (Chen et al., 2017; He & Sheffield, 2020; Marengo et al., 2013; Zscheischler et al., 2018). This phenomenon is also referred to as a spatially compounding

Supervision: Shuo Wang
Validation: Huijiao Chen
Visualization: Huijiao Chen
Writing – original draft: Huijiao Chen
Writing – review & editing: Shuo Wang, Jinxin Zhu, Dagang Wang

drought and pluvial (SCDP) event (Singh et al., 2021; Zscheischler et al., 2020). A number of real-world examples manifest the compound impacts of such concurrent extremes. In the summer of 2022, a severe drought leads to a lack of water supply in the western region of the United States while supercharged rainstorms unleash devastating flooding in Yellowstone National Park (Levitan, 2022). Multiple extreme events including record-breaking heatwave, severe drought, and deadly heavy rainfall also battered China in 2022. According to the data released by China's Ministry of Emergency Management, the drought hazard alone affected 5.527 million people and caused a direct economic loss of 395 million dollars in July of 2022 in South China. Compared with South China, a larger part of North China has experienced unusually high precipitation in July. A mountain torrent disaster induced by heavy rainfall caused many casualties on 18 August in North China. The superimposed condition of drought and flood has brought unprecedented challenges to disaster prevention, mitigation, and relief work (WMO, 2022). The simultaneous occurrence of devastating floods and severe droughts across a country might exceed the capacity of emergency management systems, and the resources needed for disaster response are inevitably strained, especially for the developing countries with limited resources.

Previous studies investigated the temporally compounding droughts and pluvials and detected their characteristics using drought indices (Chen & Wang, 2022; Dong et al., 2011; Hao et al., 2019; Trenberth et al., 2014). Nonetheless, features of spatially compounding droughts and pluvials and their dynamic evolution have seldom been addressed at large spatial scales owing to a lack of effective and reliable methods. Previous studies mainly focused on events at catchment scales (Nigam et al., 2015) or explained the historical phenomenon of "South-Flood North-Drought" (Day et al., 2018; Hao et al., 2019; Zhang et al., 2016). China is most likely to be affected by SCDP events since its climate regimes are modulated by East Asian summer monsoon and are particularly susceptible to abnormal atmospheric circulations (Day et al., 2018; Ding et al., 2008). For instance, the heatwave-induced droughts and heavy rainfall-induced pluvials may occur simultaneously across different regions in China (Chen et al., 2017). A thorough and systematic assessment of SCDP events is thus vital for better understanding their spatiotemporal dynamics and associated compound effects, thereby facilitating the sustainable development and management of water resources in China.

It is recognized that the increased volatility in precipitation is expected to amplify the spatial heterogeneity of precipitation in a warming environment (Swain et al., 2018; Wang et al., 2017; Wu et al., 2019; W. Zhang et al., 2021). It can result in a more frequent occurrence of droughts and floods under a warming condition (Chen, Wang, Zhu, &Zhang, 2020; Martin, 2018; Su et al., 2018; Wang & Wang, 2019; You & Wang, 2021; B. Zhang et al., 2021, 2022) and potentially alter the spatial pattern of SCDP events. Understanding the spatial variation in the pattern of SCDP events is thus necessary for assessing potential consequences associated with concurrent extremes. Nevertheless, little effort has been made to examine SCDP events and to assess changes in their spatial pattern from a climate projection standpoint. It is thus expected to detect changes in the characteristics of SCDP events by identifying the most fragile regions, particularly in Eastern China. Eastern China is one of the most densely populated regions around the world and is undertaking an expensive engineering project, namely the "South-North Water Transfer Project," based on the phenomenon of "South-Flood North-Drought" over the past decades.

The objective of this study is to explore the spatiotemporal evolution of boreal summer SCDP events from both historical and future perspectives over Eastern China. The high-resolution climate variables will be derived from the Climate Research Unit (CRU) data set for the historical period and four regional climate model (RCM) simulations under the Representative Concentration Pathway 8.5 (RCP 8.5) scenario. The dry and wet extremes will be identified by the self-calibrated Palmer Drought Severity Index (scPDSI). The spatiotemporal characteristics of droughts and pluvials will then be investigated by a three-dimensional (temporal–longitudinal–latitudinal) clustering approach. The changes in spatial patterns of droughts and pluvials will also be examined thoroughly to further understand the underlying mechanisms that trigger the shift pattern of SCDP events.

2. Data and Methods

2.1. Data

The Providing Regional Climate Impacts for Studies (PRECIS, Wilson et al., 2015; Zhu et al., 2018) experiment developed by the UK Hadley Centre, together with three regional climate model simulations from Coordinated Regional Climate Downscaling Experiment (CORDEX, Giorgi et al., 2012) East Asia experiments,

were used to assess the changes in the pattern of SCDP events over Eastern China. The PRECIS model was driven by the HadGEM2-ES while the three CORDEX simulations were performed by three Coupled Model Intercomparison Projection Phase 5 (CMIP5) general circulation models (CNRM-CM5, MPI-ESM-LR, and HadGEM2-ES). The horizontal resolution of the PRECIS simulation is 0.44° with the domain covering East Asia over 13.44°N–56.12°N, 64.68°E−139.04°E. The three CORDEX simulations have the same horizontal resolution of about 0.44° (~50 km). The daily 500-hPa geopotential height from the fifth generation of European ReAnalysis (ERA5 reanalysis) has a horizontal resolution of 0.25°. The monthly observed precipitation and potential evapotranspiration (PET) from gridded Climate Research Unit Time Series version 4 (CRU TS; Harris et al., 2020) were used as the observational data set with a 0.5° horizontal resolution. All four RCM simulations and the ERA5 reanalysis product were interpolated to the CRU grids for spatial comparison between simulated and observed climate variables (Table S1 in Supporting Information S1).

The 30-year monthly hydroclimatic variables, including precipitation, PET, and 500-hPa geopotential height for the historical (1975–2004) and future (2069–2098) periods, were collected from the four climate projections to assess the impacts of climate change on drought and pluvial characteristics over Eastern China and their associations with large-scale atmospheric circulations. All four RCM projections were forced with the RCP 8.5 emission scenario. The FAO-56 Penman-Monteith Equation was used for the calculation of simulated historical PET (Allen et al., 1998), while a modified PET calculation was used for the assessment of simulated PET under a warming condition (Text S1 in Supporting Information S1; Yang, Roderick, et al., 2019). We took into account possible CO_2 physiological effects on stomata resistance, which could result in a decrease in transpiration (Yang et al., 2020).

The self-calibrated Palmer Drought Severity Index (scPDSI, Palmer, 1965; Wells et al., 2004) has been widely adopted to indicate the dryness (scPDSI <= −3) and wetness (scPDSI >= +3) based on the concepts of water demand and supply, through the use of precipitation, soil characteristics, and PET (De Luca et al., 2020; Jiang et al., 2014; Yang et al., 2020). The scPDSI moisture parameter is characterized by available water content, which is derived from the State Soil Geographic Database for the top 100 cm soil profile (Liu et al., 2012). The deficit of water is the difference between actual precipitation and precipitation required to calculate the long-term monthly soil moisture (Liu et al., 2012; Wells et al., 2004). In this study, the scPDSI value of −3 was used as the threshold to identify severe dry spells, while the scPDSI value of +3 was selected as the threshold to identify severe wet spells (Table S2 in Supporting Information S1; De Luca et al., 2020).

2.2. Identification of Spatially Compounding Drought and Pluvial Events

The drought and pluvial events are identified through the Density-Based Spatial Clustering of Applications with Noise (DBSCAN) clustering algorithm. The DBSCAN clustering method is a density-based spatial clustering, which is capable of detecting the spatial and temporal drought or pluvial clusters (Joshi et al., 2013). The evolution of droughts and pluvials can be viewed as a continuum in a three-dimensional space (temporal–longitudinal–latitudinal) (Liu et al., 2019). The grid points with scPDSI values less than or equal to −3 are identified as "dryness," the grid points with scPDSI values greater than or equal to 3 are treated as "wetness," and the other grid points are classified as "normal condition."

The basic idea is that for each "drought" cluster, the neighborhood of a given radius has to have at least a minimum number of "dry" grid points (minimum area). The thresholds of radius and minimum area play a crucial role in the performance of the DBSCAN clustering algorithm. We selected 6 (May–October) as the threshold of radius and 85 grids (about 1% of the total land area) as the threshold of minimum area. These settings are consistent with previous studies related to the criteria to determine the minimum area (Liu et al., 2019; Wang et al., 2011; Xu et al., 2015), which can address the issue that a small threshold area may lead to a large-scale drought event separated into several smaller ones (Guo et al., 2018). The relatively small drought patches with an area no larger than the predetermined area threshold are ignored and are no longer included in the following process. The procedure of detecting a "pluvial" cluster is similar to the identification of a "drought" cluster.

The linkages between drought and pluvial patches mainly focus on their temporal overlap (the onset and termination of an event) (Liu et al., 2019). The drought and pluvial events might occur simultaneously across different locations over Eastern China. According to the number of droughts and pluvials occurring from May to October in each year, the matching relationships between droughts and pluvials can be divided into two categories: individual events (droughts or pluvials) and simultaneous occurrence of droughts and pluvials. Based on

10.1029/2022EF003397

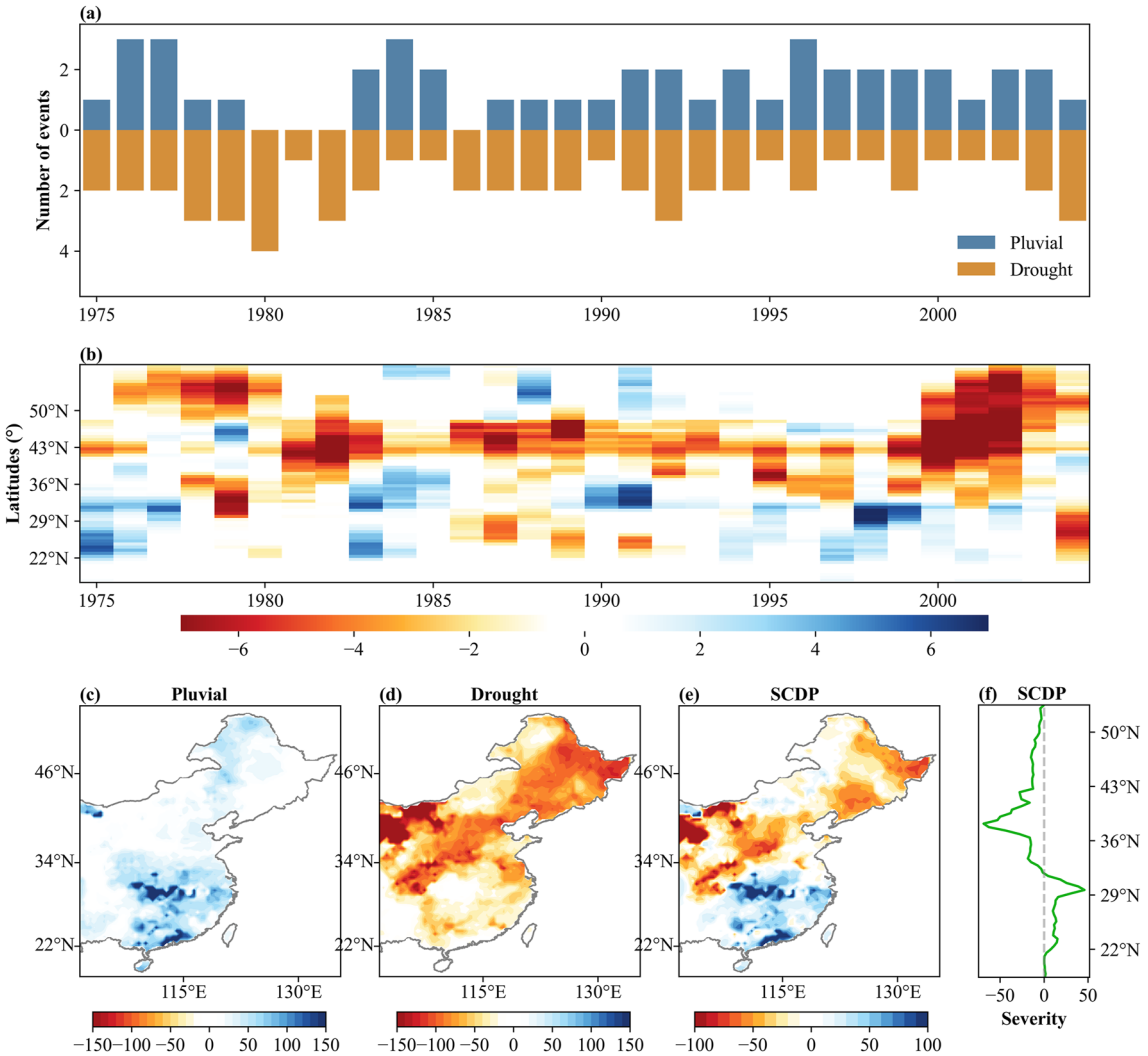

Figure 1. (a) The number of pluvials and droughts during boreal summer (May–October) from 1975 to 2004. (b) Time-latitude distribution of mean severity of pluvials and droughts. The spatial distribution of the severity of (c) pluvials, (d) droughts, and (e) SCDP events. (f) The green line represents the latitudinal mean severity of SCDP events for the historical period of 1975–2004.

these definitions, we find that Eastern China only experienced droughts for 4 years during 1975–2004 (Figure 1a) and simultaneously experienced droughts and pluvials for 26 years, which we hereafter refer to as spatially compounding drought and pluvial (SCDP) events.

We define four primary features of SCDP events: area, severity, frequency, and latitudinal mean severity. The area is defined as the fraction of land areas under drought/pluvial conditions, that is, the total number of grid cells identified as a drought/pluvial cluster. Severity is defined as the average of scPDSI values for grid cells under drought/pluvial conditions during boreal summer (May–October). Frequency is defined as the total number of years that experience the SCDP events during boreal summer. Latitudinal mean severity is defined as the latitudinal average of event severity. The observed characteristics of SCDP events were derived from the CRU data set from 1975 to 2004 with a 0.5° resolution. The changes in SCDP events were derived from four RCM simulations with the same horizontal resolution of 0.5° between the historical period of 1975–2004 and the future period of 2069–2098 under a high-emission scenario (RCP 8.5).

2.3. Significance Test

We have used year-block bootstrap resampling to estimate the significance and confidence intervals of our results. In general, we first simulated the respective variable by the year-block bootstrap resampling to generate sufficient

samples (e.g., precipitation and PET). Based on the generated samples, we then estimated uncertainties in model biases and future changes of event severity using a sign test. Finally, we applied a false detection rate to limit the false significance of the spatiotemporal relationships of gridded data.

The bootstrap resampling is widely used to estimate uncertainties in model biases or future changes due to limited sampling (Chan et al., 2020; Kendon et al., 2019; Lorenz et al., 2019). The resampling is done in yearly blocks (Chan et al., 2020; Kendon et al., 2019) to account for temporal correlation in the precipitation and PET datasets, so that we only assume independence in the respective variable for a given season between years. For all the map plots in this study, where resampling was done at each grid point, a total of $n = 100$ bootstrap samples were produced by selecting 30 years from the full data set (either historical or future model simulation) with replacement (Kendon et al., 2019). These bootstraps were used to produce 100 estimates of the difference between model simulations and observations, or between historical and future runs, generating a confidence interval for the estimated difference. Such a bootstrap resampling is able to explicitly estimate uncertainty due to the year-to-year variability (Chan et al., 2020).

Based on the samples generated from the bootstrap resampling, we carried out the two-sided sign test using the *BSDA* R package (Arnholt & Evans, 2017) to examine whether the median of the bootstrap resampling across four RCM simulations shows a significant difference in average precipitation and PET between observations and model simulations. To test for the statistical difference of the severity of pluvials, droughts, and SCDP events for each grid point, we performed the one-sided sign test using the *BSDA* R package to examine whether the median of the bootstrap resampling experiences a significant increase in the severity of events between the historical and future periods (Chiang et al., 2021).

When one conducts field significance tests, one would expect some results to be significant just by chance (Wilks, 2016). The problem can be further complicated by the inherent spatial correlation of climate data, which may lead to the incorrect identification of significant results (Renard et al., 2008; Wilk, 2016). To address this issue, the estimation of false discovery rate (Benjamini & Hochberg, 1995) is a straightforward alternative to control the expected proportion of falsely rejected null hypotheses in multiple testing, using a correction to the *p*-value (Wilks, 2016). The *p*-value corrections are implemented using the *p.adjust* in the *stats* R package or the *stats.multitest* in the *statsmodels* Python package.

3. Results

3.1. Characteristics of Historical SCDP Events

Figure 1 presents the characteristics of historical SCDP events from 1975 to 2004 in Eastern China. We find that Eastern China simultaneously experienced pluvials and droughts for 26 years during 1975–2004 (Figure 1a). Specifically, Eastern China experienced droughts in each boreal summer (May–October) and simultaneously experienced droughts and pluvials for up to 87% in a 30-year period (Figure 1a). Thus, Eastern China faces a high risk of spatial co-occurrence of droughts and pluvials during boreal summer for the historical period of 1975–2004.

Figure 1b shows the latitudinal mean severity of pluvials and droughts over Eastern China from 1975 to 2004. It is indicated that more extreme droughts occurred in Northeast China from 1999 to 2003 and in Southeast China from 1984 to 1988. The period of 1984–1988 shows the pattern of more droughts in Southeast China and more pluvials in Northeast China (DSC–PNC pattern). The period of 1999–2003 indicates the pattern of more pluvials in Southeast China and more droughts in Northeast China (PSC–DNC pattern).

The variations in the spatial relationship between pluvials and droughts are investigated using latitudinal averaged scPDSI values. The severity of droughts and pluvials shows a clear latitudinal pattern for the period of 1975–2004 (Figure 1f). A large band of positive scPDSI values in the 22°N–30°N peaks around 29°N (Figures 1c and 1f), indicating more pluvials in Southeast China (e.g., the middle and lower Yangtze River basin, Figure 1c). A band of negative scPDSI values between the 37°N–42°N peaks around 38°N (Figures 1d and 1f), showing more droughts in Northeast China (e.g., the middle Yellow River basin, Figure 1d). These results indicate the pattern of more pluvials in Southeast China and more droughts in Northeast China (PSC–DNC pattern) during the period of 1975–2004. This is in agreement with the previous studies that also reported the "Southern-Flood Northern-Drought" phenomenon over Eastern China since the late 1970s (Day et al., 2018; Ding et al., 2008; Song et al., 2014; Zhang et al., 2016).

3.2. Projected Changes in the Severity of SCDP Events

To project future changes in the severity of SCDP events relative to the historical period based on the RCM simulations, historical SCDP events were reproduced across four RCM simulations. The four RCM simulations were used to address model structural uncertainty and then were validated by comparing model outputs against observations. The multi-model ensemble (MME) median simulation can reproduce the spatial patterns of mean precipitation and PET over Eastern China even though there are significant differences in the gridded precipitation amount and PET between the MME median simulation and observations (Figures S1 and S2 in Supporting Information S1). However, there is no significant difference in the latitudinal mean amounts of precipitation and PET between the MME median simulation and observations at the 95% confidence level based on a two-sided student's *t*-test (Figure S3 in Supporting Information S1), indicating the capability of the MME in the performing a reliable assessment of key climatic variables in comparison with the CRU observation and ERA5 reanalysis over Eastern China. We used the same predefined thresholds for both the historical and future periods to make them comparable when projecting future changes in the characteristics of SCDP events. In general, there is a good agreement between RCM simulations and observations in terms of the frequency (Figure S4 in Supporting Information S1) and the spatial distribution of the severity of pluvials, droughts, and SCDP events (Figures 2a–2f). Stippling areas in Figures 2d–2f show the hot spot regions which are identified by the gridded pluvial (drought) severity greater than the 70th (less than the 30th) percentile of total pluvial (drought) severity over Eastern China based on each RCM simulation. These results demonstrate the capability of RCMs in simulating the severity of pluvials and droughts as well as identifying the "PSC–DNC" pattern from 1975 to 2004. Figures 2g–2i show the projected multi-model ensemble medians of the severity of pluvials, droughts, and SCDP events. Stippling areas in Figures 2g–2i highlight the hot spot regions which are projected to experience the most severe events. For instance, Northeast China is projected to experience more severe pluvials (Figure 2g). Meanwhile, Southeast China is expected to become more vulnerable to droughts (Figure 2h), which would reduce hydropower generation and imply that more power output is needed from other sources to meet demand.

Figure 3 shows the multi-model ensemble medians of changes in the severity of pluvials, droughts, and SCDP events. Compared to historical simulations, the severity of pluvial events is projected to increase in Northeast China (57% of Eastern China's land area; Figure 3a) but to decrease in Southeast China (38% of Eastern China's land area; Figure 3a). The severity of drought events is expected to increase in Southeast China (32% of Eastern China's land area; Figure 3b) but to decrease in Northeast China (65% of Eastern China's land area; Figure 3b). In general, there will be more intense pluvials in most parts of Northeast China, with 54% of Eastern China's land area. Meanwhile, 43% of Eastern China's land area are projected to experience more intense droughts, especially in Southeast China (Figure 3c).

Figure 3d shows the latitudinal mean severity of SCDP events for the historical period of 1975–2004 and the future period of 2069–2098. The latitudinal patterns of droughts and pluvials are projected to shift largely. Specifically, the most intense pluvials are projected to shift from Southeast China (peaks at about 29°N) to Northeast China (34°N–36°N), while the most intense droughts are projected to shift from Northeast China (37°N–42°N) to Southeast China (~22°N). These imply that a pattern of more droughts in Southeast China and more pluvials in Northeast China (DSC–PNC pattern) is expected to occur by the end of the 21st century. These results are consistent with previous findings that the consecutive dry days will decrease in the northern part of China due to the more significant precipitation increase in North China than in South China (Pan et al., 2020; Wu et al., 2019).

Figure 4 shows the multi-model ensemble medians of characteristics (frequency, affected area, and average severity) of pluvials and droughts detected for the historical and future periods. The significance of the differences between the historical and future periods is assessed using the non-parametric Mann–Whitney U test (Mann & Whitney, 1947) with 95% confidence level. The null hypothesis for this test is that no significant difference of the median characteristics between the historical and future periods. The *p*-values of frequency, affected area, and average severity of pluvials between the historical and future periods are less than 0.05 and thus the null hypothesis is rejected. We find statistically significant (p-value < 0.05) increases in spatial extent (36%) and average severity (3%) of pluvials for the future period of 2069–2098 under the RCP 8.5 scenario relative to the historical period of 1975–2004. Meanwhile, droughts are projected to be more severe and to affect more land areas over Eastern China. The frequencies of pluvials and droughts are projected to increase by 16% and 8%, respectively, contributing to an increase in the frequency of occurrence of SCDP events by the end of the 21st century relative to the historical period.

10.1029/2022EF003397

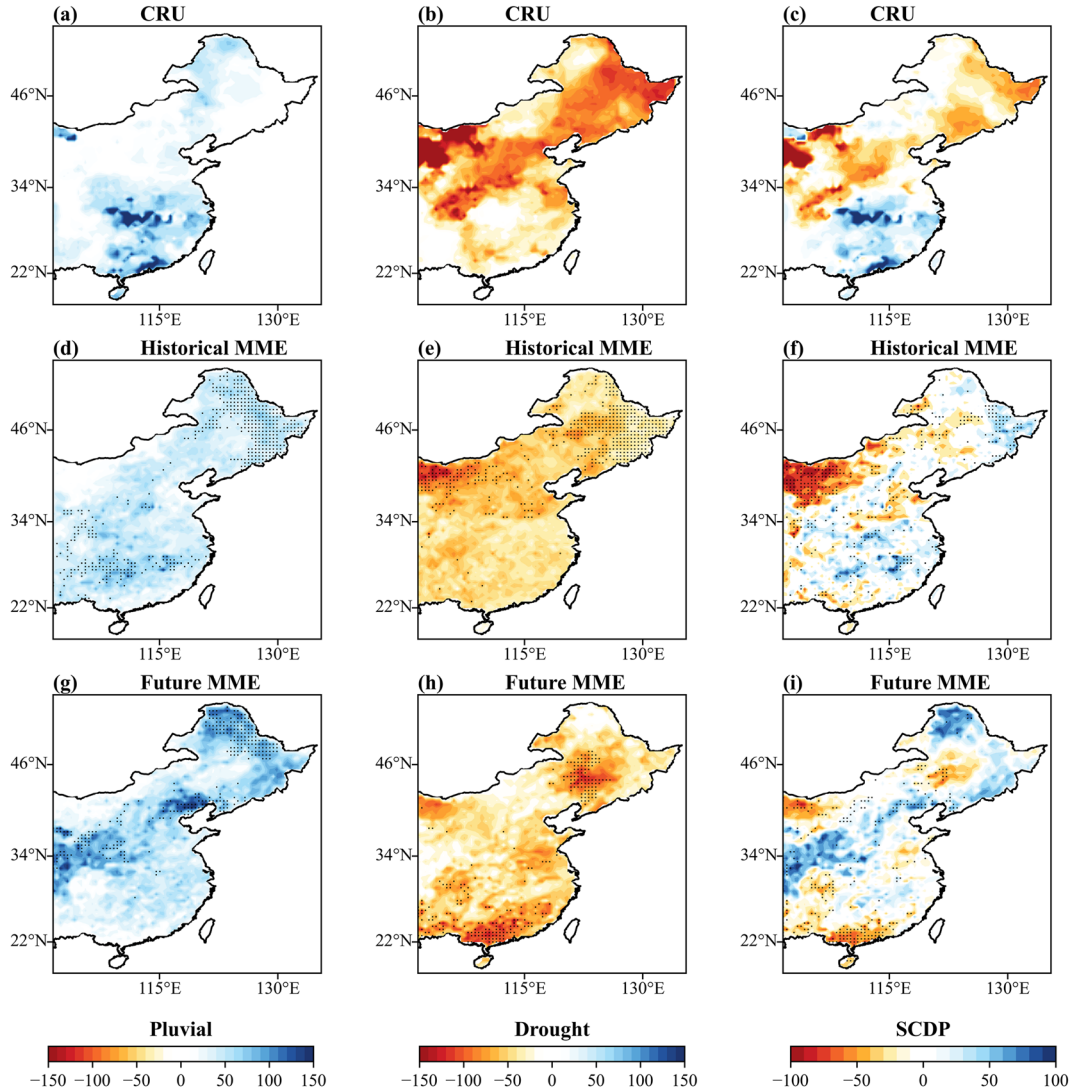

Figure 2. The severity (non-dimensional) of (a, d, and g) pluvials, (b, e, and h) droughts, and (c, f, and i) SCDP events based on the CRU observation (top row) from 1975 to 2004, historical multi-model ensemble (MME) median simulations (middle row) from 1975 to 2004, and future MME median simulations (bottom row) from 2069 to 2098. Stippling indicates that all four RCM simulations agree on the hot spot, which is identified by the gridded pluvial (drought) severity greater than the 70th (less than the 30th) percentile of total pluvial (drought) severity over Eastern China.

3.3. Potential Mechanisms Causing SCDP Events

The spatial pattern of SCDP events is modulated by thermodynamic and dynamic processes over Eastern China. The heat-induced droughts and heavy rainfall-induced pluvials owing to precipitation extremes might occur simultaneously across different regions in China, such as the summer of 2022 (WMO, 2022). There are two factors that can potentially explain the shift pattern of SCDP events.

First, the East Asia summer monsoon (EASM) influences at least half of precipitation distribution in China (Day et al., 2018; Song et al., 2014). In this study, the period of 1999–2003 shows the pattern of more pluvials in Southeast China and more droughts in Northeast China (PSC–DNC pattern), while the period of 1984–1988 indicates more droughts in Southeast China and more pluvials in Northeast China (DSC–PNC pattern), as shown in Figure 1b. Precipitation increases over Southeast China and decreases over Northeast China since the late 1970s, exhibiting a PSC–DNC pattern (e.g., 1999–2003, Figure S5a in Supporting Information S1), which is associated with the weakening of EASM circulation. By contrast, a strong EASM has been perceived as extensive southerlies inland to North China, which corresponds to the increased precipitation in Northeast China and the deficient rainfall in Southeast

10.1029/2022EF003397

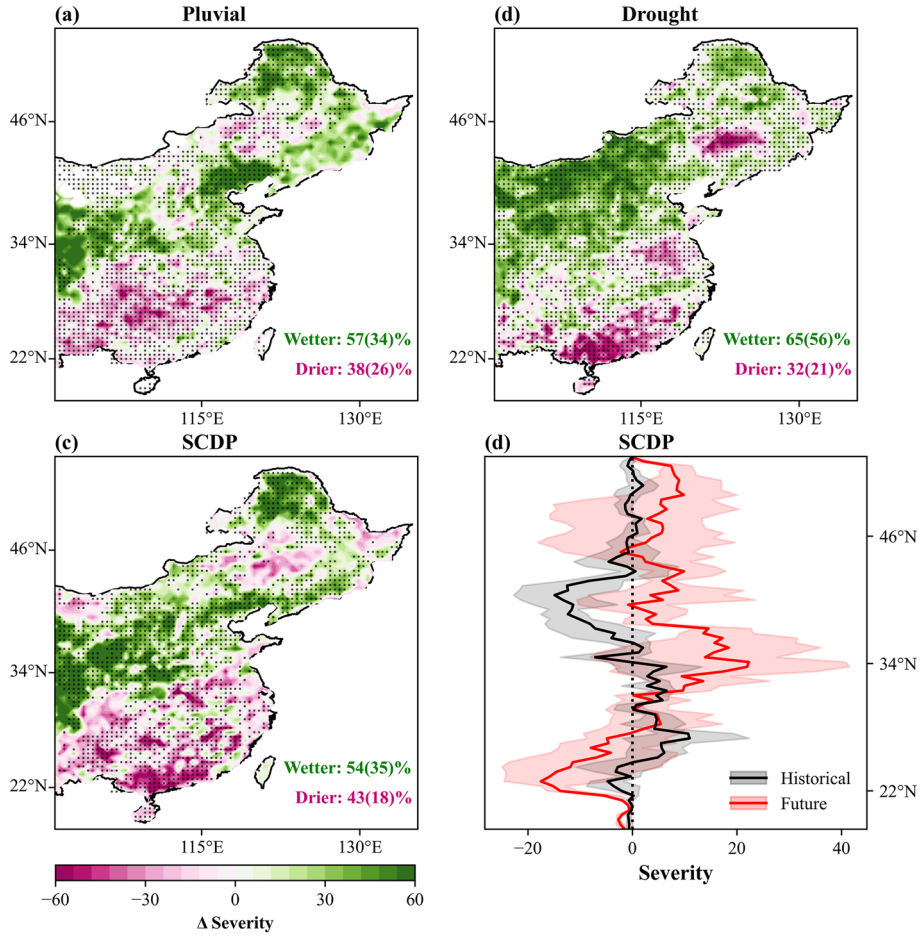

Figure 3. The changes in the severity (non-dimensional) of (a) pluvials, (b) droughts, and (c) SCDP events between the future period of 2069–2098 and the historical period of 1975–2004. (d) The black line and red line represent the latitudinal mean severity of SCDP events for the historical and future periods, respectively. The solid line represents the ensemble median and the colored shading shows the uncertainty in terms of the interquartile range across ensemble members. (a–c) The number represents the fraction of land area which is projected to experience more intense events. The number in brackets represents the fraction of land area which is projected to experience more intense events at the 95% confidence level. Stippling over each grid cell indicates a statistically significant increase in the severity of events between the historical and future periods at the 95% confidence level compared with the year-to-year variability based on a one-sided sign test. A false detection rate correction is applied to the statistical significance tests.

China (Wang et al., 2008), resulting in a DSC–PNC pattern (e.g., 1984–1988, Figure S5b in Supporting Information S1). The risk of floods and droughts during the EASM is tremendous due to the fine intra-seasonal space-time structure, coupled with the orientation of the rivers that are mostly parallel to the rain bands, triggering the occurrence of floods and droughts particularly sensitive to inter-annual variations of precipitation (Wang et al., 2008).

The summer rainfall is related to EASM over the Yangtze–Huaihe River valley in Southeast China (Ding et al., 2008; Yang, Wang, et al., 2019). Figure 5 shows the spatial pattern of the variability in summer precipitation over Eastern China for the historical period and the future period, respectively. Compared to the baseline period, the above-normal precipitation area was located in Southeast China in the historical period of 1975–2004, whereas the below-normal precipitation area was located in Northeast China (Figure 5a). The southward shift of the summer rainfall pattern over Eastern China responded to the spatial pattern of more pluvials in Southeast China and more droughts in Northeast China during 1975–2004. These findings are consistent with previous studies reporting that a weakening of EASM resulted in a southward displacement of the major monsoonal rain band since the late 1970s (Zhang et al., 2016; Zhou et al., 2009, 2020).

As for the future projection (Figure 5b), however, the above-normal rainfall zone will shift to Northeast China, while the precipitation is projected to decrease in Southeast China. A northward displacement of monsoon

10.1029/2022EF003397

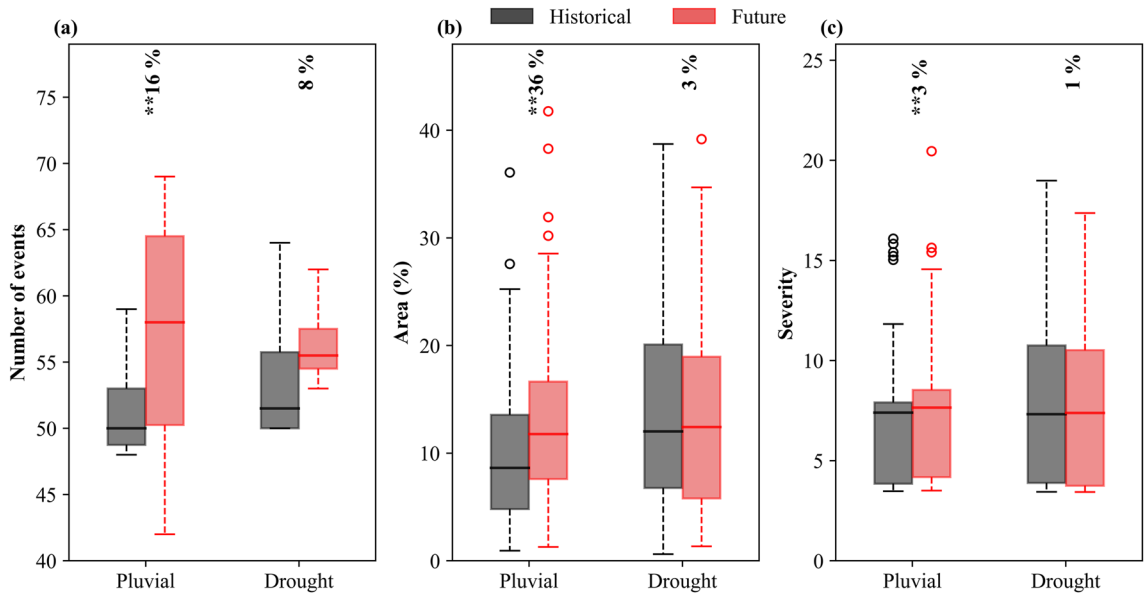

Figure 4. The boxplots of (a) the number of pluvials and droughts for the historical (1975–2004) and the future (2069–2098) periods based on four RCM simulations. (b–c) The distribution of affected areas and average severity of pluvials and droughts associated with SCDP events. The number above the boxplot indicates the percentage increase in (a) frequency, (b) fraction of affected land areas, and (c) average severity. "**" at the top of the panel indicates that the medians of frequency, affected area, or average severity of events are significantly different between the historical and future periods at the 95% confidence level using a Mann–Whitney U test.

rain belt (Yang et al., 2015) may contribute to the pluvial-dominant regime toward Northeast China and the drought-dominant regime shifts toward Southeast China under a warming climate. The location of monsoon rain belt is regulated by many factors, including the Sea Surface Temperature (Liu et al., 2021), the western Pacific subtropical High (WPSH; Hsu et al., 2017; Zhang et al., 2016), the boreal summer intra-seasonal oscillation (Chen et al., 2017), and the El Niño-Southern Oscillation (Hao et al., 2019), which all may affect the shift pattern of SCDP events over Eastern China.

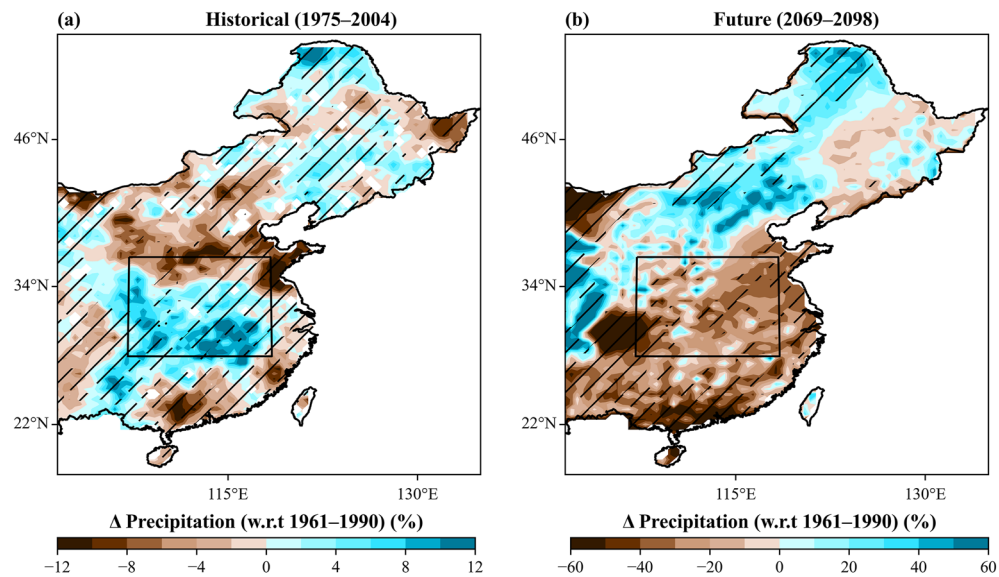

Figure 5. The changes in mean precipitation anomalies (mm/month) during boreal summer (May–October) for (a) the historical period (1975–2004) and (b) the future period (2069–2098) relative to the baseline period (1961–1990), respectively. The black rectangle represents the Yangtze-Huaihe River valley in Eastern China where summer precipitation is highly related to the East Asia summer monsoon (Yang, Wang, et al., 2019). Stippling indicates that the differences between two periods are statistically significant at the 95% confidence level compared with the year-to-year variability based on a one-sided sign test. A false detection rate correction is applied to the statistical significance tests.

10.1029/2022EF003397

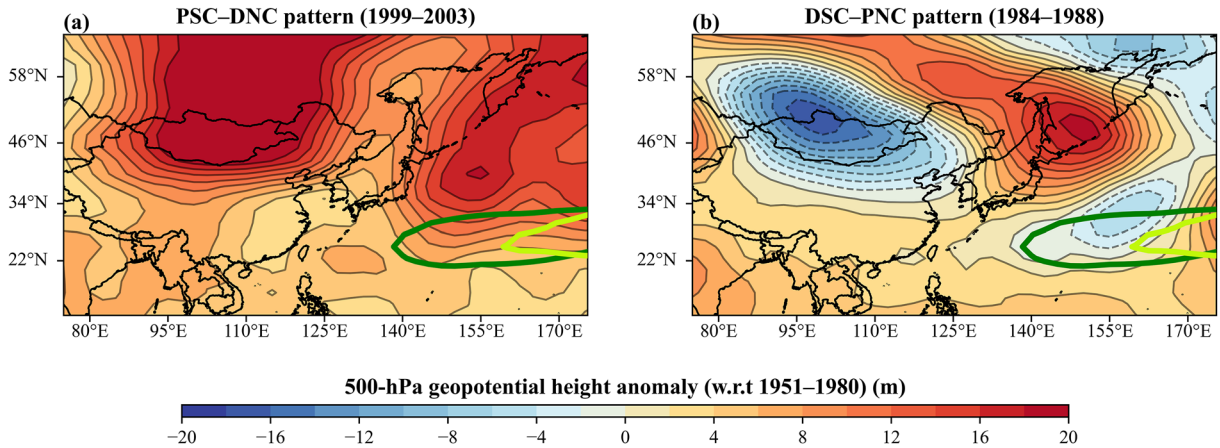

Figure 6. Composite differences of 500-hPa geopotential height (m) during June–August (a) between the period of 1999–2003 and the reference period of 1951–1980 as well as (b) between the period of 1984–1988 and the reference period of 1951–1980 based on ERA5 reanalysis. Dark green and light green represent the 5880-m contour of 500-hPa geopotential height during June–August for the period of 1999–2003 and the period of 1984–1988, respectively.

Second, there is a strong correlation between the WPSH and SCDP events during the summer over Eastern China. The low-level southwesterly jet at the northwestern edge of the WPSH transports a large amount of water vapor into China (Guan et al., 2019; Zhou & Yu, 2005). The location and intensity of the WPSH could regulate the position of summer precipitation in Eastern China due to the interplay between monsoonal warm air and cold air from middle or high latitudes (Chaluvadi et al., 2021; Day et al., 2018; Guan et al., 2019; Zhou & Yu, 2005).

The geopotential height at 500-hPa over China shows a significant difference between the PSC–DNC and DSC–PNC patterns (Figure 6). Positive geopotential height anomalies occur in China at 500-hPa during the period of 1999–2003 and the strength of the WPSH is much stronger for the PSC–DNC pattern (Figure 6a). As for the DSC–PNC pattern, the WPSH becomes very weak, and the spatial pattern of droughts and pluvials presents an opposite trend (Figure 6b). Zhang et al. (2016) suggested that the WPSH plays a key role in the spatial pattern of droughts and floods over Eastern China, which agrees well with our results.

Figures 7a and 7b indicate a westward extension and stronger intensity of WPSH in the recent period of 1975–2004, compared to the reference period of 1951–1980, which is consistent with previous studies (Wu & Wang, 2015; Zhou et al., 2009). A stronger WPSH intensity results in enhanced southwesterly airflow and transports more water vapor from the South China Sea, which in turn leads to more precipitation in Southeast China (Zhao & Wang, 2017). As most of the rainfall occurs in South China due to the enhanced southwesterly transport of moisture, water vapor is largely depleted in air masses transported toward North China, resulting in dry and hot conditions over Northeast China under a strong WPSH (Zhao & Wang, 2017).

Figure 7c shows the changes in the strength of WPSH under the RCP 8.5 scenario (See Text S2 and Figure S6 in Supporting Information S1 for historical evaluations of WPSH indices). The negative changes in 500-hPa geopotential height (Figure 7c) almost cover the entire western North Pacific, representing a weakening or eastward retreat of the WPSH in response to global warming. The spatial pattern of changes in the geopotential height (Figure 7c) is similar to that of the regressed eddy geopotential height indicated by previous studies (He et al., 2018; Zhou et al., 2020). We find that the DSC–PNC pattern for the future period of 2069–2098 might respond to a weaker or eastward retreat of the WPSH under the RCP 8.5 scenario. He et al. (2015) suggested that the WPSH tended to weaken and retreat eastward under the RCP 8.5 scenario due to a weakened meridional temperature gradient in the mid-troposphere. Consequently, the weakening strength of the WPSH and a northward displacement of the monsoon rain belt may contribute to the pluvial-dominant regime shifts toward Northeast China and the drought-dominant regime shifts toward Southeast China under a warming climate.

4. Discussion

We explore the evolution of SCDP events based on different settings of the proposed framework. This framework consists of various components, including the definition of drought and pluvial events based on the scPDSI

10.1029/2022EF003397

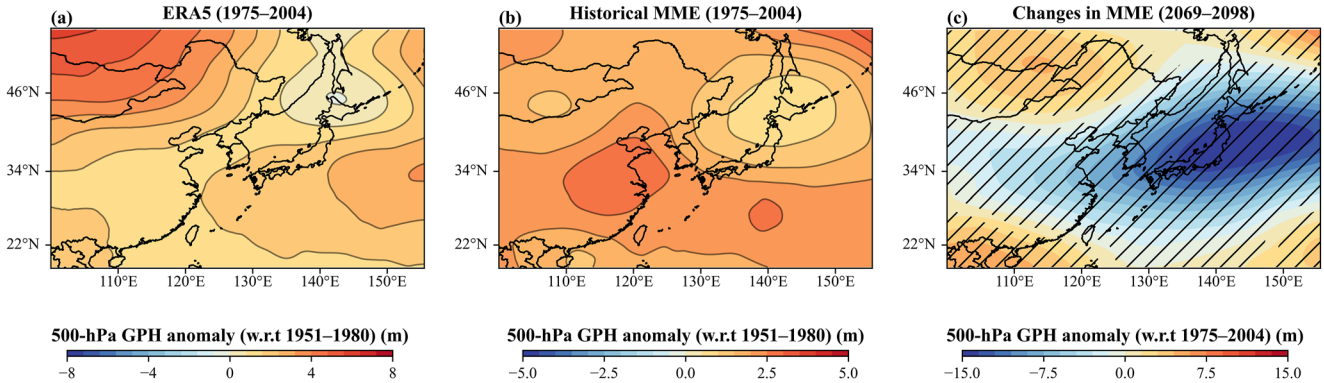

Figure 7. Climatological summer median of the 500-hPa geopotential height anomalies (GPH, m) during 1975–2004 (w.r.t 1951–1980) based on (a) the EAR5 reanalysis and (b) the multi-model ensemble (MME) median simulations. (c) Future changes in summer 500-hPa geopotential height anomalies for the future period of 2069–2098 relative to the historical period of 1975–2004. Stippling indicates that the medians of future changes are statistically significant at the 95% confidence level compared with the year-to-year variability based on a one-sided sign test. A false detection rate correction is applied to the statistical significance tests.

thresholds, radius, and minimum area, for detecting SCDP events. First, the scPDSI values of −3 and 3 are used to identify the severity of droughts and pluvials, respectively (De Luca et al., 2020). As expected, an increased number of years that experience the SCDP events can be detected by the relatively small thresholds (e.g., the values of −2 and 2). The values of −4 and 4 are too strict to obtain sufficient samples for analyzing the statistics of droughts and pluvials (Figure S7 in Supporting Information S1).

The thresholds of the radius and the minimum area play a crucial role in the performance of the DBSCAN clustering algorithm. Thus, a sensitivity assessment was performed to examine the influence of these thresholds on the latitudinal mean severity of SCDP events (Figure S8 in Supporting Information S1) The use of the threshold value of a radius smaller than 3 and more than 7 cannot identify any drought or pluvial event. In addition, the relatively mild events with an affected area of no more than 50 grids are neglected due to the fact that such events can hardly cause devastating damages. We selected 6 (May–October) as the threshold of radius and 85 grids (about 1% of the total land area) as the threshold of minimum area. These settings are consistent with previous studies related to the criteria to determine the minimum area (Liu et al., 2019; Wang et al., 2011; Xu et al., 2015), which can address the issue that a small threshold area may lead to a large-scale drought event separated into several smaller ones (Guo et al., 2018). Different thresholds of radius and minimum area were used to examine the shift pattern of SCDP events, which show a consistent result (Figure S8 in Supporting Information S1). Overall, various thresholds and their combinations were used in this study to detect SCDP events and to correctly reconstruct a spatial pattern of PSC–DNC in the historical period and a shift pattern of DSC–PNC in the future period, improving the robustness and reliability of our findings.

The SCDP events were detected using a three dimensional temporal–longitudinal–latitudinal identification approach (DBSCAN clustering algorithm). Compared to the commonly used Empirical Orthogonal Function (EOF) method, the three-dimensional clustering algorithm has the following advantages. First, the DBSCAN clustering can provide more accurate location and time information of disasters for urgent responses (Singh et al., 2017; Yu et al., 2020), by straightforwardly exhibiting the development and evolution of droughts and pluvials. Second, the spatial-temporal distribution patterns and dynamics of spatially compounding drought and pluvial events can be captured from a three-dimensional perspective, facilitating a more in-depth analysis of mechanisms behind the spatial co-occurrence of extreme events. Nonetheless, the three-dimensional clustering algorithm has limitations. For instance, mild droughts or pluvials are excluded using the clustering algorithm, potentially resulting in an underestimation of droughts and pluvials.

5. Conclusion

In this study, we explore the spatiotemporal evolution of SCDP events over Eastern China. Historical spatial patterns of SCDP events are investigated based on the CRU data set, and their future changes are projected using the multi-model regional climate simulations under the RCP 8.5 scenario, advancing our understanding of the underlying mechanisms that trigger the SCDP events under a warming climate.

Our findings reveal that Eastern China faces a high risk of spatial co-occurrence of devastating drought and severe pluvial events. Eastern China is projected to simultaneously experience more frequent and more intense pluvials and droughts with larger affected land areas as the climate warms. A prominent pattern of more pluvials in Southeast China and more droughts in Northeast China is investigated for the past 30 years. The severity of droughts is projected to increase in Southeast China and the severity of pluvials is expected to increase in Northeast China under a warming climate. Thus, the pattern of SCDP events is expected to dynamically evolve: the pluvial-dominated regime shifts from Southeast to Northeast China, while the drought-dominated regime moves from Northeast to Southeast China. This shift pattern may be attributed to the weakening strength of the WPSH and a northward displacement of the monsoon rain belt.

It should be noted that the short-duration drought and pluvial events are not considered because the scPDSI represents water deficits at a medium scale (H. Zhao et al., 2017). Moreover, the clustering algorithm (DBSCAN) was used in this study to identify drought and pluvial events from a three-dimensional perspective, but our analysis did not account for the uncertainty of different clustering algorithms. It is thus expected to take into account different sources of uncertainty, including algorithms and emission scenarios, to further improve the robustness of our analysis. A further investigation of the thermodynamic and dynamic processes is also needed to improve the understanding of physical mechanisms behind the spatial co-occurrence of dry and wet extremes.

Data Availability Statement

The gridded monthly precipitation and PET can be accessible in (a) the Climatic Research Unit Time Series version 4.00: https://data.ceda.ac.uk/badc/cru/data/cru_ts/ and (b) the three Coordinated Regional Climate Downscaling Experiment East Asia experiments: https://esg-dn1.nsc.liu.se/projects/cordex/. (c) The gridded monthly 500-hPa geopotential height can be accessible in ERA5 reanalysis: https://cds.climate.copernicus.eu/cdsapp#!/dataset/reanalysis-era5-pressure-levels-monthly-means?tab=overview. (d) The scPDSI datasets can be available in https://data.mendeley.com/datasets/43z87by5gg/4.

Acknowledgments
This research was supported by the National Natural Science Foundation of China (Grant 51809223), the Hong Kong Research Grants Council Early Career Scheme (Grant 25222319), and the RILS Strategic Supporting Scheme (Grant P0043040).

References

Allen, R., Pereira, L., Raes, D., & Smith, M. (1998). Crop evapotranspiration: Guidelines for computing crop water requirements-FAO irrigation and drainage paper 56. *Fao Rome*, *9*, 300.

Arnholt, A. T., & Evans, B. (2017). BSDA: Basic statistics and data analysis.

Benjamini, Y., & Hochberg, Y. (1995). Controlling the false discovery rate: A practical and powerful approach to multiple testing. *Journal of the Royal Statistical Society: Series B*, *57*(1), 289–300. https://doi.org/10.1111/j.2517-6161.1995.tb02031.x

Chaluvadi, R., Varikoden, H., Mujumdar, M., & Ingle, S. (2021). Variability of west Pacific subtropical high and its potential importance to the Indian summer monsoon rainfall. *International Journal of Climatology*, *41*(7), 4047–4060. https://doi.org/10.1002/joc.7057

Chan, S. C., Kendon, E. J., Berthou, S., Fosser, G., Lewis, E., & Fowler, H. J. (2020). Europe-wide precipitation projections at convection permitting scale with the Unified Model. *Climate Dynamics*, *55*(3–4), 409–428. https://doi.org/10.1007/s00382-020-05192-8

Chen, H., & Wang, S. (2022). Accelerated transition between dry and wet periods in a warming climate. *Geophysical Research Letters*, *49*(19), e2022GL099766. https://doi.org/10.1029/2022GL099766

Chen, H., Wang, S., & Wang, Y. (2020). Exploring abrupt alternations between wet and dry conditions on the basis of historical observations and convection-permitting climate model simulations. *Journal of Geophysical Research: Atmospheres*, *125*(9), 1–17. https://doi.org/10.1029/2019JD031982

Chen, H., Wang, S., Zhu, J., & Zhang, B. (2020). Projected changes in abrupt shifts between dry and wet extremes over China through an ensemble of regional climate model simulations. *Journal of Geophysical Research: Atmospheres*, *125*(29), e2020JD033894. https://doi.org/10.1029/2020JD033894

Chen, Y., Zhai, P., & Li, L. (2017). Low-frequency oscillations of East Asia/Pacific teleconnection and simultaneous weather anomalies/extremes over eastern Asia. *International Journal of Climatology*, *37*(1), 276–295. https://doi.org/10.1002/joc.4703

Chiang, F., Mazdiyasni, O., & AghaKouchak, A. (2021). Evidence of anthropogenic impacts on global drought frequency, duration, and intensity. *Nature Communications*, *12*(1), 2754. https://doi.org/10.1038/s41467-021-22314-w

Day, J., Fung, I., & Liu, W. (2018). Changing character of rainfall in eastern China, 1951−2007. *Proceedings of the National Academy of Sciences of the United States of America*, *115*(9), 2016–2021. https://doi.org/10.1073/pnas.1715386115

De Luca, P., Messori, G., Wilby, R. L., Mazzoleni, M., & Di Baldassarre, G. (2020). Concurrent wet and dry hydrological extremes at the global scale. *Earth System Dynamics*, *11*(1), 251–266. https://doi.org/10.5194/esd-11-251-2020

Ding, Y., Wang, Z., & Sun, Y. (2008). Inter-decadal variation of the summer precipitation in East China and its association with decreasing Asian summer monsoon. Part I: Observed evidences. *International Journal of Climatology*, *28*(9), 1139–1161. https://doi.org/10.1002/joc.1615

Dong, X., Xi, B., Kennedy, A., Feng, Z., Entin, J. K., Houser, P. R., et al. (2011). Investigation of the 2006 drought and 2007 flood extremes at the Southern Great Plains through an integrative analysis of observations. *Journal of Geophysical Research*, *116*(3), D03204. https://doi.org/10.1029/2010JD014776

Duan, W., Zou, S., Christidis, N., Schaller, N., Chen, Y., Sahu, N., et al. (2022). Changes in temporal inequality of precipitation extremes over China due to anthropogenic forcings. *NPJ Climate and Atmospheric Science*, *5*(1), 1–13. https://doi.org/10.1038/s41612-022-00255-5

Giorgi, F., Coppola, E., Solmon, F., Mariotti, L., Sylla, M. B., Bi, X., et al. (2012). RegCM4: Model description and preliminary tests over multiple CORDEX domains. *Climate Research*, *52*(1), 7–29. https://doi.org/10.3354/cr01018

Guan, W., Hu, H., Ren, X., & Yang, X. (2019). Subseasonal zonal variability of the western Pacific subtropical high in summer: Climate impacts and underlying mechanisms. *Climate Dynamics*, *53*(5–6), 3325–3344. https://doi.org/10.1007/s00382-019-04705-4

Guo, H., Bao, A., Ndayisaba, F., Liu, T., Jiapaer, G., El-Tantawi, A. M., & De Maeyer, P. (2018). Space-time characterization of drought events and their impacts on vegetation in Central Asia. *Journal of Hydrology*, *564*, 1165–1178. https://doi.org/10.1016/j.jhydrol.2018.07.081

Hao, Z., Sun, D., Wu, M., & Zheng, J. (2019). Does El Niño play an early signal role for the south-flood north-drought pattern over eastern China? *Theoretical and Applied Climatology*, *137*(1–2), 217–227. https://doi.org/10.1007/s00704-018-2590-6

Harris, I., Osborn, T. J., Jones, P., & Lister, D. (2020). Version 4 of the CRU TS monthly high-resolution gridded multivariate climate dataset. *Scientific Data*, *7*(1), 1–18. https://doi.org/10.1038/s41597-020-0453-3

He, C., Lin, A., Gu, D., Li, C., Zheng, B., Wu, B., & Zhou, T. (2018). Using eddy geopotential height to measure the western North Pacific subtropical high in a warming climate. *Theoretical and Applied Climatology*, *131*(1), 681–691. https://doi.org/10.1007/s00704-016-2001-9

He, C., Zhou, T., Lin, A., Wu, B., Gu, D., Li, C., & Zheng, B. (2015). Enhanced or weakened western North Pacific subtropical high under global warming? *Scientific Reports*, *5*(1), 1–7. https://doi.org/10.1038/srep16771

He, X., & Sheffield, J. (2020). Lagged compound occurrence of droughts and pluvials globally over the past seven decades. *Geophysical Research Letters*, *47*(14), e2020GL087924. https://doi.org/10.1029/2020gl087924

Hsu, P., Lee, J., Ha, K., & Tsou, C. (2017). Influences of boreal summer intraseasonal oscillation on heat waves in monsoon Asia. *Journal of Climate*, *30*(18), 7191–7211. https://doi.org/10.1175/JCLI-D-16-0505.1

Jiang, R., Xie, J., He, H., Luo, J., & Zhu, J. (2014). Use of four drought indices for evaluating drought characteristics under climate change in Shaanxi, China: 1951–2012. *Natural Hazards*, *75*(3), 2885–2903. https://doi.org/10.1007/s11069-014-1468-x

Joshi, D., Samal, A., & Soh, L. K. (2013). Spatio-temporal polygonal clustering with space and time as first-class citizens. *GeoInformatica*, *17*(2), 387–412. https://doi.org/10.1007/s10707-012-0157-8

Kendon, E. J., Stratton, R. A., Tucker, S., Marsham, J. H., Berthou, S., Rowell, D. P., & Senior, C. A. (2019). Enhanced future changes in wet and dry extremes over Africa at convection-permitting scale. *Nature Communications*, *10*(1), 1794. https://doi.org/10.1038/s41467-019-09776-9

Levitan, D. (2022). Welcome to the summer from hell: 2022 is shaping up to be a season of disaster — And a preview of our future. *Grid*. https://www.grid.news/story/climate/2022/06/24/welcome-to-the-summer-from-hell-2022-is-shaping-up-to-be-a-season-of-disaster-and-a-preview-of-our-future/

Liu, H., Feng, X., Tao, A., & Zhang, W. (2021). Intraseasonal variability of sea level in the Western North Pacific. *Journal of Geophysical Research: Oceans*, *126*(6). https://doi.org/10.1029/2021JC017237

Liu, L., Hong, Y., Bednarczyk, C., Yong, B., Shafer, M., Riley, R., & Hocker, J. (2012). Hydro-climatological drought analyses and projections using meteorological and hydrological drought indices: A case study in Blue River basin, Oklahoma. *Water Resources Management*, *26*(10), 2761–2779. https://doi.org/10.1007/s11269-012-0044-y

Liu, Y., Zhu, Y., Ren, L., Singh, V. P., Yong, B., Jiang, S., et al. (2019). Understanding the spatiotemporal links between meteorological and hydrological droughts from a three-dimensional perspective. *Journal of Geophysical Research: Atmospheres*, *124*(6), 3090−3109–3109. https://doi.org/10.1029/2018JD028947

Lorenz, R., Stalhandske, Z., & Fischer, E. M. (2019). Detection of a climate change signal in extreme heat, heat stress, and cold in Europe from observations. *Geophysical Research Letters*, *46*(14), 8363–8374. https://doi.org/10.1029/2019GL082062

Mann, H. B., & Whitney, D. R. (1947). On a test of whether one of two random variables is stochastically larger than the other. *The Annals of Mathematical Statistics*, *18*(1), 50–60. https://doi.org/10.1214/aoms/1177730491

Marengo, J., Alves, L., Soares, W., Rodriguez, D., Camargo, H., Riveros, M., & Pabló, A. (2013). Two contrasting severe seasonal extremes in tropical South America in 2012: Flood in Amazonia and drought in northeast Brazil. *Journal of Climate*, *26*(22), 9137−9154–9154. https://doi.org/10.1175/JCLI-D-12-00642.1

Martin, E. (2018). Future projections of global pluvial and drought event characteristics. *Geophysical Research Letters*, *45*(21), 11913–11920. https://doi.org/10.1029/2018GL079807

Nigam, S., Zhao, Y., Ruiz-Barradas, A., & Zhou, T. (2015). The south-flood north-drought pattern over eastern China and the drying of the Gangetic Plain. In C. P. Chang (Ed.), *Climate chang: Multidecadal and beyond* (pp. 347–359). World Scientific. https://doi.org/10.1142/9789814579933_0022

Palmer, W. (1965). *Meteorological drought*. U.S. Weather Bureau. Research Paper No.45.

Pan, X., Zhang, L., & Huang, C. (2020). Future climate projection in northwest China with RegCM4.6. *Earth and Space Science*, *7*(2), 1–18. https://doi.org/10.1029/2019EA000819

Qing, Y., Wang, S., Ancell, B., & Yang, Z. (2022). Accelerating flash droughts induced by the joint influence of soil moisture depletion and atmospheric aridity. *Nature Communications*, *13*(1), 1139. https://doi.org/10.1038/s41467-022-28752-4

Renard, B., Lang, M., Bois, P., Dupeyrat, A., Mestre, O., Niel, H., et al. (2008). Regional methods for trend detection: Assessing field significance and regional consistency. *Water Resources Research*, *44*(8), W08419. https://doi.org/10.1029/2007WR006268

Schumann, G., Frye, S., Wells, G., Adler, R., Brakenridge, R., Bolten, J., et al. (2016). Unlocking the full potential of Earth observation during the 2015 Texas flood disaster. *Water Resources Research*, *52*(5), 3288–3293. https://doi.org/10.1002/2015WR018428

Singh, J., Ashfaq, M., Skinner, C., Anderson, W., & Singh, D. (2021). Amplified risk of spatially compounding droughts during co-occurrences of modes of natural ocean variability. *NPJ Climate and Atmospheric Science*, *4*(1), 1–14. https://doi.org/10.1038/s41612-021-00161-2

Singh, J., Dwivedi, Y., Rana, N., Kumar, A., & Kapoor, K. (2017). Event classification and location prediction from tweets during disasters. *Annals of Operations Research*, *283*(1–2), 737–757. https://doi.org/10.1007/s10479-017-2522-3

Song, F., Zhou, T., & Qian, Y. (2014). Responses of East Asian summer monsoon to natural and anthropogenic forcings in the 17 latest CMIP5 models. *Geophysical Research Letters*, *41*(2), 596–603. https://doi.org/10.1002/2013GL058705

Su, B., Huang, J., Fischer, T., Wang, Y., Kundzewicz, Z., Zhai, J., et al. (2018). Drought losses in China might double between the 1.5°C and 2.0°C warming. *Proceedings of the National Academy of Sciences of the United States of America*, *115*(42), 10600–10605. https://doi.org/10.1073/pnas.1802129115

Swain, D., Langenbrunner, B., Neelin, J., & Hall, A. (2018). Increasing precipitation volatility in twenty-first-century California. *Nature Climate Change*, *8*(5), 427–433. https://doi.org/10.1038/s41558-018-0140-y

Trenberth, K., Dai, A., Van Der Schrier, G., Jones, P., Barichivich, J., Briffa, K., & Sheffield, J. (2014). Global warming and changes in drought. *Nature Climate Change*, *4*(1), 17–22. https://doi.org/10.1038/nclimate2067

UNDRR, & CRED. (2019). An overview of the last 20 years the last 20 years.

Wang, A., Lettenmaier, D., & Sheffield, J. (2011). Soil moisture drought in China, 1950–2006. *Journal of Climate*, *24*(13), 3257–3271. https://doi.org/10.1175/2011JCLI3733.1

Wang, B., Wu, Z., Li, J., Liu, J., Chang, C., Ding, Y., & Wu, G. (2008). How to measure the strength of the East Asian summer monsoon. *Journal of Climate*, *21*(17), 4449–4463. https://doi.org/10.1175/2008JCLI2183.1

Wang, G., Wang, D., Trenberth, K., Erfanian, A., Yu, M., Bosilovich, M., & Parr, D. (2017). The peak structure and future changes of the relationships between extreme precipitation and temperature. *Nature Climate Change*, *7*(4), 268–274. https://doi.org/10.1038/nclimate3239

Wang, S., & Wang, Y. (2019). Improving probabilistic hydroclimatic projections through high-resolution convection-permitting climate modeling and Markov chain Monte Carlo simulations. *Climate Dynamics*, *53*(3), 1613–1636. https://doi.org/10.1007/s00382-019-04702-7

Wells, N., Goddard, S., & Hayes, M. (2004). A self-calibrating palmer drought severity index. *Journal of Climate*, *17*(12), 2335–2351. https://doi.org/10.1175/1520-0442(2004)017<2335:ASPDSI>2.0.CO;2

Wilks, D. (2016). The stippling shows statistically significant grid points": How research results are routinely overstated and over interpreted, and what to do about it. *Bulletin of the American Meteorological Society*, *97*(12), 2263–2273. https://doi.org/10.1175/BAMS-D-15-00267.1

Wilson, W., Hassell, D., Hein, D., Wang, C., Tucker, S., Jones, R., & Taylor, R. (2015). Technical manual for PRECIS: The met office Hadley Centre regional climate modelling system version 2.0.0.

WMO. (2022). Extreme weather in China highlights climate change impacts and need for early warnings. Retrieved from https://public.wmo.int/en/media/news/extreme-weather-china-highlights-climate-change-impacts-and-need-early-warnings

Wu, L., & Wang, C. (2015). Has the western Pacific subtropical high extended westward since the late 1970s? *Journal of Climate*, *28*(13), 5406–5413. https://doi.org/10.1175/JCLI-D-14-00618.1

Wu, S., Wu, Y., & Wen, J. (2019). Future changes in precipitation characteristics in China. *International Journal of Climatology*, *39*(8), 3558–3573. https://doi.org/10.1002/joc.6038

Xu, K., Yang, D., Yang, H., Li, Z., Qin, Y., & Shen, Y. (2015). Spatio-temporal variation of drought in China during 1961–2012: A climatic perspective. *Journal of Hydrology*, *526*, 253–264. https://doi.org/10.1016/j.jhydrol.2014.09.047

Yang, S., Ding, Z., Li, Y., Wang, X., Jiang, W., & Huang, X. (2015). Warming-induced northwestward migration of the East Asian monsoon rain belt from the Last Glacial Maximum to the mid-Holocene. *Proceedings of the National Academy of Sciences of the United States of America*, *112*(43), 13178–13183. https://doi.org/10.1073/pnas.1504688112

Yang, Y., Roderick, M., Zhang, S., McVicar, T., & Donohue, R. (2019). Hydrologic implications of vegetation response to elevated CO_2 in climate projections. *Nature Climate Change*, *9*(1), 44–48. https://doi.org/10.1038/s41558-018-0361-0

Yang, Y., Wang, H., Chen, F., Zheng, X., Fu, Y., & Zhou, S. (2019). TRMM-based optical and microphysical features of precipitating clouds in summer over the Yangtze–Huaihe River valley, China. *Pure and Applied Geophysics*, *176*(1), 357–370. https://doi.org/10.1007/s00024-018-1940-8

Yang, Y., Zhang, S., Roderick, M., McVicar, T., Yang, D., Liu, W., & Li, X. (2020). Comparing palmer drought severity index drought assessments using the traditional offline approach with direct climate model outputs. *Hydrology and Earth System Sciences*, *24*(6), 2921–2930. https://doi.org/10.5194/hess-24-2921-2020

You, J., & Wang, S. (2021). Higher probability of occurrence of hotter and shorter heat waves followed by heavy rainfall. *Geophysical Research Letters*, *48*(17), e2021GL094831. https://doi.org/10.1029/2021GL094831

Yu, M., Bambacus, M., Cervone, G., Clarke, K., Duffy, D., Huang, Q., et al. (2020). Spatiotemporal event detection: A review. *International Journal of Digital Earth*, *13*(12), 1339–1365. https://doi.org/10.1080/17538947.2020.1738569

Zhang, B., Wang, S., & Wang, Y. (2021). Probabilistic projections of multidimensional flood risks at a convection-permitting scale. *Water Resources Research*, *57*(1), 1–28. https://doi.org/10.1029/2020wr028582

Zhang, B., Wang, S., & Zhu, J. (2022). A weighted ensemble of regional climate projections for exploring the spatiotemporal evolution of multi-dimensional drought risks in a changing climate. *Climate Dynamics*, *58*(1–2), 49–68. https://doi.org/10.1007/s00382-021-05889-4

Zhang, W., Furtado, K., Wu, P., Zhou, T., Chadwick, R., Marzin, C., et al. (2021). Increasing precipitation variability on daily-to-multiyear time scales in a warmer world. *Science Advances*, *7*(31), 1–12. https://doi.org/10.1126/sciadv.abf8021

Zhang, Z., Jin, Q., Chen, X., Xu, C. Y., & Jiang, S. (2016). On the linkage between the extreme drought and pluvial patterns in China and the large-scale atmospheric circulation. *Advances in Meteorology*, *2016*, 1–12. https://doi.org/10.1155/2016/8010638

Zhao, H., Gao, G., An, W., Zou, X., Li, H., & Hou, M. (2017). Timescale differences between SC-PDSI and SPEI for drought monitoring in China. *Physics and Chemistry of the Earth*, *102*, 48–58. https://doi.org/10.1016/j.pce.2015.10.022

Zhao, Z., & Wang, Y. (2017). Influence of the west Pacific subtropical high on surface ozone daily variability in summertime over eastern China. *Atmospheric Environment*, *170*, 197–204. https://doi.org/10.1016/j.atmosenv.2017.09.024

Zhou, S., Huang, G., & Huang, P. (2020). Inter-model spread of the changes in the East Asian summer monsoon system in CMIP5/6 models. *Journal of Geophysical Research: Atmospheres*, *125*(24), 2020JD033016. https://doi.org/10.1029/2020JD033016

Zhou, T., & Yu, R. (2005). Atmospheric water vapour transport associated with typical anomalous summer rainfall patterns in China. *Journal of Geophysical Research*, *110*(D8), D08104. https://doi.org/10.1029/2004JD005413

Zhou, T., Yu, R., Zhang, J., Drange, H., Cassou, C., Deser, C., et al. (2009). Why the western Pacific subtropical high has extended westward since the late 1970s. *Journal of Climate*, *22*(8), 2199–2215. https://doi.org/10.1175/2008JCLI2527.1

Zhu, J., Huang, G., Wang, X., Cheng, G., & Wu, Y. (2018). High-resolution projections of mean and extreme precipitations over China through PRECIS under RCPs. *Climate Dynamics*, *50*(11), 4037–4060. https://doi.org/10.1007/s00382-017-3860-1

Zscheischler, J., Martius, O., Westra, S., Bevacqua, E., Raymond, C., Horton, R., et al. (2020). A typology of compound weather and climate events. *Nature Reviews Earth & Environment*, *1*(7), 333–347. https://doi.org/10.1038/s43017-020-0060-z

Zscheischler, J., Westra, S., Hurk, J. M. B., Seneviratne, S., Ward, P., Pitman, A., et al. (2018). Future climate risk from compound events. *Nature Climate Change*, *8*(6), 469–477. https://doi.org/10.1038/s41558-018-0156-3